REPORT DOCUMENTATION PAGE

AFRL-SR-BL-TR-01-

0268

1. AGENCY USE ONLY (Leave blank)	2. REPORT DATE	3. REPORT TYPE AND DATES COVERED
		Final: 01 February 98 – 31 May 01

4. TITLE AND SUBTITLE

Simulation and Modeling of Wind Effects on Airdrop Systems

5. FUNDING NUMBERS

F 49620-98-1-0214

6. AUTHOR(S)

Michael L. Accorsi & John W. Leonard – University of Connecticut
Tayfun E. Tezduyar – Rice University

7. PERFORMING ORGANIZATION NAME(S) AND ADDRESS(ES)

Dept. of Civil & Environmental Engr.
University of Connecticut
Storrs, CT 06269-2037

Mechanical Engr. and Materials Science
Rice University - MS 321
6100 Main Street
Houston, TX 77005-1892

8. PERFORMING ORGANIZATION REPORT NUMBER

9. SPONSORING / MONITORING AGENCY NAME(S) AND ADDRESS(ES)

AFOSR/NA
110 Duncan Avenue, Room B115
Bolling AFB, DC 20332-8050

10. SPONSORING / MONITORING

20020118 017

11. SUPPLEMENTARY NOTES

The views, opinions and/or findings contained in this report are those of the author(s) and should not be construed as
An official AFOSR position, policy, or decision, unless so designated by other documentation.

RESEARCH (AFOSR)
THIS TECHNICAL REPORT
HAS BEEN REVIEWED AND IS APPROVED FOR PUBLIC RELEASE
DISTRIBUTION IS UNLIMITED.

12a. DISTRIBUTION / AVAILABILITY STATEMENT

Approved for public release; distribution unlimited

12b. DISTRIBUTION CODE

13. ABSTRACT *(Maximum 200 Words)*

The goal of this project has been to develop computational tools for the simulation of candidate airdrop systems for the New World Vistas (NWV) Precision Airdrop (PAD) program. To accomplish this goal, researchers from the University of Connecticut, Rice University, and the US Army Soldier Systems Center at Natick have collaborated in developing a coupled Computational Fluid Dynamics (CFD) and Structural Dynamics (CSD) program to simulate three-dimensional, transient Fluid-Structure Interaction (FSI) phenomena for airdrop systems.

The work performed under this project consists of (1) development of new CFD methods, (2) development of new CSD methods, (3) development of new methods for coupled FSI simulations, (4) verification of the FSI model, and (5) simulation of candidate NWV airdrop systems. The FSI simulations require large scale, nonlinear, transient finite element models for the parachute system and surrounding airflow and therefore are computationally intensive. To address this difficulty, parallel computational techniques have been developed for the FSI model.

14. SUBJECT TERMS			15. NUMBER OF PAGES
			16. PRICE CODE
17. SECURITY CLASSIFICATION OF REPORT	18. SECURITY CLASSIFICATION OF THIS PAGE	19. SECURITY CLASSIFICATION OF ABSTRACT	20. LIMITATION OF ABSTRACT
UNCLASSIFIED	UNCLASSIFIED	UNCLASSIFIED	UL

Simulation and Modeling of Wind Effects on Airdrop Systems

1. FORWARD

The goal of this project has been to develop computational tools for the simulation of candidate airdrop systems for the New World Vistas (NWV) Precision Airdrop (PAD) program. To accomplish this goal, researchers from the University of Connecticut, Rice University, and the US Army Soldier Systems Center at Natick have collaborated in developing a coupled Computational Fluid Dynamics (CFD) and Structural Dynamics (CSD) program to simulate three-dimensional, transient Fluid-Structure Interaction (FSI) phenomena for airdrop systems.

The work performed under this project consists of (1) development of new CFD methods, (2) development of new CSD methods, (3) development of new methods for coupled FSI simulations, (4) verification of the FSI model, and (5) simulation of candidate NWV airdrop systems. The FSI simulations require large scale, nonlinear, transient finite element models for the parachute system and surrounding airflow and therefore are computationally intensive. To address this difficulty, parallel computational techniques have been developed for the FSI model.

The CFD model is based on the Deforming-Spatial-Domain/Stabilized-Space-Time (DSD/SST) formulation developed by the Team for Advanced Flow Simulation and Modeling (T*AFSM) at Rice University. The CSD model is based on the Total Lagrange formulation for geometrically nonlinear dynamic behavior of flexible membranes and cables developed by the University of Connecticut. The coupled FSI method was developed by Natick and Rice University in collaboration with the University of Connecticut.

2. TABLE OF CONTENTS

3. LIST OF APPENDIXES

- Appendix A:

Selected Publications
1. Structural Modeling of Parachute Dynamics
2. Fluid-Structure Interaction Modeling of the US Army Personnel Parachute System

4. PROBLEM STATEMENT

The primary goal of this project has been to develop computational tools for the simulation of candidate airdrop systems for the New World Vistas (NWV) Precision Airdrop (PAD) program. The computational methods require the coupling of a Computational Structural Dynamics (CSD) model for the parachute system with a Computational Fluid Dynamics (CFD) model for the surrounding airflow to perform Fluid-Structure Interaction (FSI) simulations. To accomplish this goal, the following specific problems in each area must be addressed:

Computational Structural Dynamics

- *A robust structural model is required to simulate the transient, geometrically nonlinear behavior of thin membrane and cable structures.* Parachute systems undergo highly transient behavior with large relative motion. Robust algorithms are required to maintain stability of the numerical solution and accurately simulate this complex behavior.

- *A rigorous method is needed to model the loss of tension in fabric membrane structures such as parachute canopies.* Fabric structures do not support compressive stresses and undergo "wrinkling" at the onset of compression. Since the behavior of a structure will differ dramatically depending on whether there is compression or no-compression, it is necessary to account for wrinkling in parachute systems.

- *Special CSD models are needed to model Pneumatic Muscle Actuators (PMAs) for simulation of NWV candidate systems.* PMAs are the primary control device being used in the NWV PAD program. PMAs utilize a braided fiber cylinder that undergoes large relative motions under rapid pressurization. A geometrically nonlinear formulation for PMAs is required.

- *Stand-alone CSD simulations are needed to verify the structural model and to provide a preliminary modeling capability for candidate NWV systems.* Stand-alone CSD simulations with approximate fluid loads (prescribed pressure and velocity dependent drag)

Computational Fluid Dynamics

- *A robust fluid dynamics model is required to simulate flow fields that involve moving boundaries and interface.* For the CFD model, it is necessary to solve the time-dependent, 3D Navier-Stokes equations for incompressible flow. Additionally, the CFD model must account for the moving boundary corresponding to the parachute canopy.

- *Sophisticated mesh generation algorithms are needed to automatically generate and update the CFD mesh with moving boundaries and interfaces.* As the parachute system deforms and travels through the fluid medium, the fluid mesh must conform to the moving boundary.

- *Computational methods are needed to simulate the effects of adverse wind fields on parachute systems.* The CFD model must also include a general method to prescribe wind conditions on the parachute model.

- *Stand-alone CFD simulations are needed to verify the fluid dynamics model.* To verify the CFD model, stand-alone simulations are performed with prescribed structural geometry.

Fluid-Structure Interaction

- *A robust method is required to couple the CSD and CFD to perform FSI simulations.* FSI simulations require the interchange of data between the CSD and CFD models. Specifically, the CSD model must pass the structural displacements and velocities to the CFD model and the CFD model must pass the fluid pressures to the CFD model. This data interchange occurs for each time step and an iterative coupling scheme is required to insure convergence of the FSI model.

5. SUMMARY OF RESULTS

The goal of this project has been to develop computational tools for the simulation of candidate airdrop systems for the New World Vistas (NWV) Precision Airdrop (PAD) program. To achieve this goal, the following results were completed:

- The CSD, CFD, and FSI models were formulated and implemented in a parallel computational environment.

- A robust CSD model was formulated and implemented. A new wrinkling algorithm was implemented in the CSD model. Details of the wrinkling algorithm and numerical results are given in References [1] and [2].

- A method for modeling PMAs was formulated and implemented. The PMA is treated as a geometrically nonlinear anisotropic membrane. Details of this formulation and numerical results are given in References [3] and [4].

- Stand-alone CSD simulations representative of NWV PAD airdrop systems were performed to verify the CSD model. Numerical results from these simulations are given in References [5] and [6].

- The CFD model uses the Deforming-Spatial-Domain / Stabilized Space Time (DSD/SST) formulation developed by the Team for Advanced Flow Simulation and Modeling (T*AFSM) at Rice University. This approach is ideally suited for parachute problems since they require modeling of a moving boundary in the flow field. Details of this formulation are given in References [7] and [8].

- A formulation for coupling the CSD and CFD models to perform FSI simulations was developed and implemented. The formulation uses a tight coupling scheme that iterates on the CSD and CFD solutions at each time step to converge on the coupled solution. Details of this formulation and simulation results are given in References [9] and [10] .

- The FSI model was validated by comparison of simulation results with wind tunnel measurements. Agreement between the simulation results and measurements was very good. Results from this validation study are given in Reference [11].

- FSI simulations were performed on candidate systems to evaluate the ability to control these systems using prescribed riser length changes. The candidate systems included both T-10 and G-12 canopies. Results from these simulations for the T-10 canopy are given in References [12] and [13].

- A major difficulty was encountered in performing FSI simulations with control operations. The control operations typically result in large distortion of the inflated canopy accompanied by contact between adjacent gores. This difficulty is illustrated in Figures 1 and 2.

- The large distortion of the canopy and contact of adjacent gores generally resulted in failure of the CFD model due to gross distortion of the CFD mesh. A method to overcome this difficulty was not developed during the project duration and this became the most limiting factor for performing additional FSI simulations.

- Our research team will continue to perform FSI simulations of NWV PAD airdrop systems under a three-year DoD Challenge Project titled "*Airdrop System Modeling for the 21st Century Airborne Warrior*".

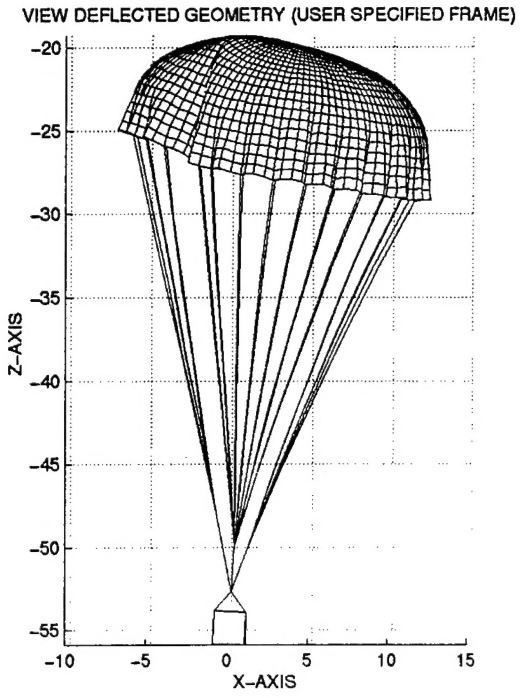

Figure 1: Deformed Configuration with Control Operation

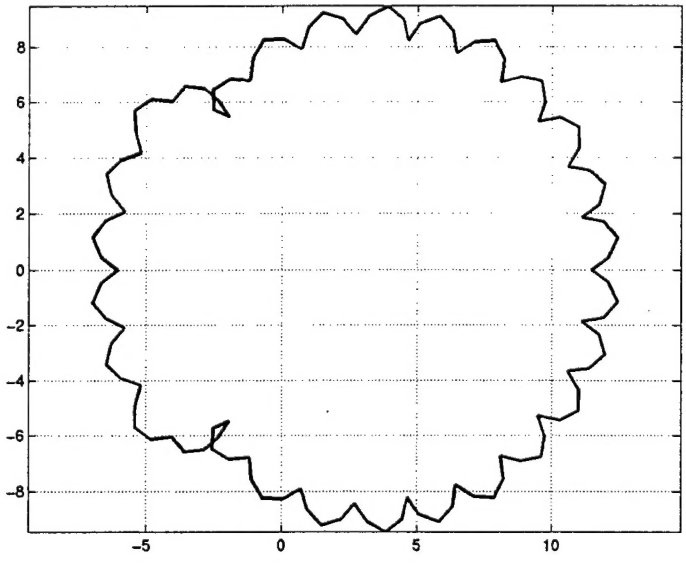

Figure 2: Skirt Profile with Gore Contact

References

1. K. Lu, M. Accorsi, and J. Leonard (2001) "Finite Element Analysis of Membrane Wrinkling," *International Journal for Numerical Methods in Engineering* **50**, 1017-1038.

2. M. Accorsi, K. Lu, J. Leonard, R. Benney and K. Stein (1999) "Issues in Parachute Structural Modeling: Damping and Wrinkling," 15th CEAS/AIAA Aerodynamic Decelerator Systems Technology Conference, June, 1999, Toulouse, France.

3. M. Gupta, Z. Xu, W. Zhang, M. Accorsi, J. Leonard, R. Benney, and K. Stein, (2001) "Recent Advances in Structural Modeling of Parachute Dynamics," AIAA-2001-2030, 16th AIAA Aerodynamic Decelerator Systems Technology Conference, May 2001, Boston MA.

4. W. Zhang, (2001) "Parallel Finite Element Methods for the Simulation of Parachute Dynamics and Control," Ph.D. Dissertation, University of Connecticut, October 2001.

5. M.L. Accorsi, J.W. Leonard, R. Benney, and K.Stein, (2000) "Structural Modeling of Parachute Dynamics," *AIAA Journal,* **38**, 139-146.

6. R. Benney, K. Stein, W. Zhang, M. Accorsi and J. Leonard (1999) "Controllable Airdrop Simulations Utilizing a 3-D Structural Dynamics Model," 15th CEAS/AIAA Aerodynamic Decelerator Systems Technology Conference, June, 1999, Toulouse, France.

7. T. Tezduyar, M. Behr, and J. Liou, (1992) "A New Strategy for Finite Element Computations Involving Moving Boundaries and Interfaces – The Deforming-Spatial-Domain/Space-Time Procedure: I. The Concept and the Preliminary Tests," *Computer Methods in Applied Mechanics and Engineering*, **94**, 339-351.

8. T. Tezduyar, M. Behr, S. Mittal, and J. Liou, (1992) "A New Strategy for Finite Element Computations Involving Moving Boundaries and Interfaces – The Deforming-Spatial-Domain/Space-Time Procedure: II. Computation of Free-Surface Flows, Two-Liquid Flows, and Flows with Drifting Cylinders," *Computer Methods in Applied Mechanics and Engineering*, **94**, 353-371.

9. K. Stein (2000) "Simulation and Modeling Techniques for Parachute Fluid-Structure Interactions," Ph.D. Dissertation, University of Minnesota, December 1999.

10. K. Stein, R. Benney, V. Kalro, T. Tezduyar, J.W. Leonard, and M.L. Accorsi (2000) "Parachute Fluid Structure Interactions: 3-D Computation," *Computer Methods in Applied Mechanics and Engineering* **190**, 373-386.

11. K. Stein, R. Benney, V. Kalro, T. Tezduyar, T. Bretl and J. Potvin, (1999) "Fluid-Structure Interaction Simulations of a Cross-Parachute: Comparison of Numerical Predictions with Wind Tunnel Data," 15th CEAS/AIAA Aerodynamic Decelerator Systems Technology Conference, AIAA-1999-1725, Toulouse, 1999.

12. K. Stein, R. Benney, T. Tezduyar, M. Accorsi, and J. Leonard, (2000) "Fluid-Structure Interaction Modeling of the US Army Personnel Parachute System" AIAA GN&C Conference, August 2000, Denver, Colorado.

13. K. Stein, R. Benney, V. Kalro, T. Tezduyar, J. Leonard and M. Accorsi (1999) "3-D Computation of Parachute Fluid-Structure Interactions: Performance and Control," 15th CEAS/AIAA Aerodynamic Decelerator Systems Technology Conference, June 1999, Toulouse, France.

7. SCIENTIFIC PERSONNEL

- Principal Investigators
  Professor John W. Leonard, University of Connecticut
  Professor Michael L. Accorsi, University of Connecticut
  Professor Tayfun Tezduyar, Rice University

- Graduate Students
  Wenqing Zhang , Ph.D., University of Connecticut
  Vinay Kalro, Ph.D. University of Minnesota
  Vinod Kumar, Ph.D. Rice University
  Yasuo Osawa, Ph.D. Rice University

- Collaborators
  Mr. Richard Benney, US Army Soldier Systems Center
  Dr. Keith Stein, US Army Soldier Systems Center

8. INVENTIONS

- No inventions were conceived during this research project.

9. APPENDIX A

Selected Publications
1. Structural Modeling of Parachute Dynamics
2. Fluid-Structure Interaction Modeling of the US Army Personnel Parachute System

AIAA JOURNAL
Vol. 37, No. 9, September 1999

Structural Modeling of Parachute Dynamics

Michael Accorsi* and John Leonard†
University of Connecticut, Storrs, Connecticut 06269-2037
and
Richard Benney‡ and Keith Stein‡
U.S. Army Soldier and Biological Chemical Command, Natick, Massachusetts 01760-5017

The dynamic behavior of parachute systems is an extremely complex phenomena characterized by nonlinear, time-dependent coupling between the parachute and surrounding airflow, large shape changes in the parachute, and three-dimensional unconstrained motion of the parachute through the fluid medium. Because of these complexities, the design of parachutes has traditionally been performed using a semi-empirical approach. This approach to design is time consuming and expensive. The ability to perform computer simulations of parachute dynamics would significantly improve the design process and ultimately reduce the cost of parachute system development. The finite element formulation for a structural model capable of simulating parachute dynamics is presented. Explicit expressions are given for structural mass and stiffness matrices and internal and external force vectors. Algorithms for solution of the nonlinear dynamic response are also given. The capabilities of the structural model are demonstrated by three example problems. In these examples, the effect of the surrounding airflow is approximated by prescribing the canopy pressure and by applying cable and payload drag forces on the structural model. The examples demonstrate the ability to simulate three-dimensional unconstrained dynamics beginning with an unstressed folded configuration corresponding to the parachute cut pattern. The examples include simulations of the inflation, terminal descent, and control phases.

Nomenclature

${}'A, A$	= determinant of metric tensors ${}'A_{\alpha\beta}$ and $A_{\alpha\beta}$, respectively
${}'A_{\alpha\beta}, A_{\alpha\beta}$	= covariant metric tensors of $'C$ and $^\circ C$, respectively
${}'A^{\alpha\beta}, A^{\alpha\beta}$	= contravariant metric tensors of $'C$ and $^\circ C$, respectively
$C^{\alpha\beta\lambda\mu}$	= material constitutive tensor
${}'D_{Ni}$	= Cartesian displacements of node N on element from $^\circ C$ to $'C$
$\dot{D}_{Ni}$	= Cartesian velocities of node N on element in $'C$
$\ddot{D}_{Ni}$	= Cartesian accelerations of node N on element in $'C$
$\{{}^\#D\}, \{{}^\#\tilde{D}\}$	= correct and estimated displacement vector of nodes from $^\circ C$ to $'C$, respectively
E	= Young's modulus
$\hat{e}_i$	= unit base vectors in Cartesian directions
e_{ijk}	= permutation symbol
${}'F_{Ni}$	= discretized external force on node N
$H_N(x_\alpha)$	= polynomial shape function of x_α
h	= thickness of membrane
$[K_{\text{eff}}]$	= effective stiffness matrix for Newmark method
$[{}^\#K]$	= estimated tangent stiffness matrix on ${}^\#C$
M_{MNij}	= mass matrix connecting nodes M and N
${}'\hat{N}$	= unit normal to $'C$
${}'n^{\alpha\beta}, {}^\#n^{\alpha\beta}$	= Kirchhoff stress resultant tensors on $'C$ and ${}^\#C$, respectively
p	= net pressure on canopy
${}'p_i$	= Cartesian components of tractions on $'C$
${}'R_{Ni}$	= discretized internal restoring force on node N
t	= time
${}'u_i$	= Cartesian displacements of point to $'C$ from $^\circ C$
${}'\ddot{u}_i$	= Cartesian accelerations of point to $'C$ from $^\circ C$
x_α	= nondimensional curvilinear coordinates in element
$\tilde{Y}_{Ni}$	= Cartesian coordinates of node N on element in $^\circ C$
y_i	= Cartesian coordinates of a point on $^\circ C$
${}'y_i$	= Cartesian coordinates of a point on $'C$
α, β	= Newmark parameters
${}'\gamma_{\alpha\beta}$	= Green strain tensor
$\{{}^\#\Delta D\}$	= correction vector to estimate $\{{}^\#\tilde{D}\}$
Δt	= time step
δ_{ij}	= Kronecker delta
δu_i	= virtual displacements
η, λ	= damping parameters
ν	= Poisson's ratio
ξ, ω	= damping ratio and natural frequency of a particular mode of free vibration
ρ	= mass density of $^\circ C$

I. Introduction

PARACHUTE deployment, inflation, and terminal descent are extremely difficult aerodynamic phenomena to model. These processes are governed by coupled, nonlinear, time-dependent equations for the interaction of the fluid medium and parachute. Because of these complexities, it is not surprising that the design of parachutes has historically been performed using semi-empirical methods.[1]

During the last two decades, the demands placed on parachute designers have increased tremendously. Payload costs have increased, mission requirements have become more stringent, and the flight tests needed to design new parachute systems have become more costly. In light of these demands, the traditional semi-empirical approach to parachute design is inadequate. Computational methods have the greatest potential for providing the necessary predictive models for parachute design.

The three phases that occur during a parachute mission are deployment, inflation, and terminal descent with precision soft landing.[2] The deployment phase is a highly nonlinear process in which the parachute and suspension lines unfold from the deployment bag. In the inflation phase, airflow causes large canopy shape changes as the parachute is stressed and begins to decelerate. This phase is also highly nonlinear, and maximum forces typically occur during this time. The terminal descent phase corresponds to all behavior following inflation and may include various control operations performed on the parachute system. In general, all three phases involve strong coupling between the parachute system and surrounding airflow.

Received 1 October 1998; revision received 5 May 1999; accepted for publication 11 May 1999.

*Associate Professor, Department of Civil and Environmental Engineering; accorsi@engr.uconn.edu.
†Professor, Department of Civil and Environmental Engineering.
‡Aerospace Engineer, Soldier Systems Center.

Computer simulations of all three phases are needed to fully characterize the behavior of a given parachute system under given conditions. In general, comprehensive simulations require coupling of structural dynamics (SD) and computational fluid dynamic (CFD) models to capture the true aerodynamic behavior, however, valuable information can be obtained from either standalone SD or CFD simulations. The finite element method (FEM) is most commonly used for the SD model and grid-based CFD and vortex element methods are both used for fluid modeling. Standalone SD simulations are performed by prescribing the canopy pressure and aerodynamic drag on the parachute components and are computationally efficient because the SD model is usually considerably smaller than the required CFD model. For standalone CFD simulations, the parachute geometry is prescribed, and the surrounding airflow is calculated. The calculated surface loads are then used to derive global parachute motion.

II. Previous Work

Deployment has been successfully simulated by Purvis[3] using a discrete element model similar to Sundberg.[4] In that axisymmetric model, the partially deployed canopy and suspension lines are modeled as elastically connected, lumped mass nodes, and semiempirical parameters account for aerodynamic forces. Although improvements to this model are possible, three-dimensional finite element modeling of the initial deployment process have not yet been performed.

Significant progress has recently been made on simulation of the parachute inflation and terminal descent phases. Coupled inflation simulations of axisymmetric parachutes have been presented by Haug et al.[5] and Stein et al.[6] Three-dimensional standalone SD inflation simulations have been presented by Mosseev[7] and Benney et al.[8] Standalone CFD models have been used to predict the flowfield in the terminal descent phase surrounding a canopy with prescribed geometry. This type of analysis has been performed for round parachutes,[9] round parachute clusters,[10] and parafoils.[11,12] Standalone SD simulations of cross and round parachutes and parafoils in terminal descent have been demonstrated by Benney et al.[8] Coupled simulations of the terminal descent phase beginning with an inflated canopy shape have recently been performed by Nelsen,[13] Stein et al.,[14] and Benney et al.[15]

In summary, the ability to perform standalone SD inflation simulations has been demonstrated by several researchers. Standalone CFD predictions of the flowfield surrounding a parachute with a prescribed rigid shape are generally available. Coupled dynamic and deformable inflation simulations have been very limited. Coupled simulations of the terminal descent phase beginning with an inflated canopy shape have recently been achieved by several researchers. To date, detailed simulation of the initial deployment phase has not been addressed. There still exists a tremendous need to perform coupled dynamic simulations of all three phases of a parachute dynamics problem.

The purpose of this paper is to present the theoretical foundations for an SD model capable of simulating parachute deployment, inflation, and terminal descent. This model is being developed jointly by researchers at the U.S. Army Soldier Systems Command, Natick Research, Development, and Engineering Center, and the University of Connecticut, and a parallel version of the model is being coupled with a CFD model developed by researchers at the Army High Performance Computing Research Center at Rice University. The structural theory has been incorporated into a finite element code that is highly tailored for parachute simulations. Several standalone SD simulations are presented to demonstrate the capabilities of this structural code. The example problems are rather complex, and corresponding experimental data is not readily available. The predictions of the coupled model have recently been compared with experiments and good agreement was obtained.[16]

III. SD Theory

In this section we consider the nonlinear dynamic behavior of thin, extremely flexible, and cable-reinforced membranes using the FEM.[17,18] Isoparametric elements[19] are used to develop discretized equations of motion admitting large dynamic displacements. A total Lagrangian[19] coordinate system is adopted, with curvilinear local coordinates embedded in the reference surface. The nonlinear dynamic responses are integrated in time using an implicit Newmark method.[19]

In the following, capital Latin letters as indices denote nodal variables on an element. Greek indices take on the values 1 and 2 on the surface, and lower case Latin indices take on the values 1, 2, and 3. A repeated index indicates summation over the range of the index. Commas used as subscripts denote partial differentiation with respect to the coordinate component with the succeeding index. A special notation is adopted to identify various configurations of the membrane: A leading superscript on a variable denotes the surface on which the variable is defined. The reference surface where magnitudes and orientations of the variables are defined is the initial unstrained state ${}^{\circ}C$. Thus, we will arrive at a total Lagrangian description of the nonlinear equations at time t on surface ${}^{t}C$, or at time $t + \Delta t$ on ${}^{t+\Delta t}C$.

A. Geometric Interpolation

The simultaneous interpolation of geometry as well as displacements by the same shape functions, that is, isoparametric interpolation, can be used for curved cables and membranes. We specify curvilinear coordinates x_1 and x_2 on the reference surface ${}^{\circ}C$ to be nondimensional natural coordinates and assume the Cartesian coordinates y_i and displacements ${}^{t}u_i$ at a generic point in the element to be given by

$$y_i(x_\alpha) = H_N(x_\alpha) Y_{iN} \tag{1a}$$

$${}^{t}u_i(x_\alpha) = H_N(x_\alpha)\, {}^{t}D_{iN} \tag{1b}$$

where $H_N(x_\alpha)$ are the element shape functions. We adopt polynomial shape functions that map a general quadrilateral or triangular surface element curved in three-dimensional space onto two-dimensional squares or triangles.

As the surface of the membrane deforms from the unstrained state ${}^{\circ}C$ to ${}^{t}C$ at time t we write the time-varying coordinates as

$${}^{t}y_i = y_i + {}^{t}u_i \tag{2a}$$

Because the metric tensor of a differential arc length in ${}^{t}C$ relative to ${}^{\circ}C$ is given by[20] [using Eqs. (1)]

$${}^{t}A_{\alpha\beta} = {}^{t}y_{i,\alpha} \cdot {}^{t}y_{i,\beta} = H_{N,\alpha} H_{M,\beta} (Y_{iN} + {}^{t}D_{iN})(Y_{iM} + {}^{t}D_{iM}) \tag{2b}$$

and because the Green strain tensor[20] of a differential arc length on ${}^{t}C$ relative to ${}^{\circ}C$ is

$${}^{t}\gamma_{\alpha\beta} = \frac{{}^{t}A_{\alpha\beta} - A_{\alpha\beta}}{2}$$

$$= H_{N,\alpha} H_{M,\beta} \frac{Y_{iN}\, {}^{t}D_{iM} + Y_{iM}\, {}^{t}D_{iN} + {}^{t}D_{iN}\, {}^{t}D_{iM}}{2} \tag{3}$$

the stress resultant tensor for a Hookean material is

$${}^{t}n^{\alpha\beta} = C^{\alpha\beta\lambda\mu}\, {}^{t}\gamma_{\lambda\mu} \tag{4}$$

where for an isotropic material in plane stress[20]

$$C^{\alpha\beta\lambda\mu} = \frac{hE\nu}{(1-\nu^2)} A^{\alpha\beta} A^{\lambda\mu} + \frac{hE}{2(1+\nu)} (A^{\alpha\lambda} A^{\beta\mu} + A^{\alpha\mu} A^{\beta\lambda}) \tag{5}$$

B. Equations of Motion

We will develop the discretized equations of motion in terms of an arbitrary constitutive equation that will allow several existing material models to be used; Eq. (5) is a particular example. The equations of motion can be developed from the principle of virtual work as written on the dynamic equilibrium state ${}^{t}C$ but referred to ${}^{\circ}C$ as[17]

$$0 = \int\int ({}^{t}n^{\alpha\beta} \delta\gamma_{\alpha\beta} - {}^{t}p_i \delta u_i) \sqrt{A}\, \mathrm{d}x_1\, \mathrm{d}x_2$$

$$+ h \int\int \rho\, {}^{t}\ddot{u}_i \delta u_i \sqrt{A}\, \mathrm{d}x_1\, \mathrm{d}x_2 \tag{6}$$

where $\delta\gamma_{\alpha\beta}$ is the infinitesimal virtual strain corresponding to a small virtual displacement δu_i superposed on $'C$, and the force vector

$$\bar{F}\sqrt{'A}\,dx_1\,dx_2 = {}'p_i\sqrt{A}\,dx_1\,dx_2\hat{e}_i \tag{7}$$

has been expressed in terms of Cartesian components $'p_i$.

In a consistent mass approach, the accelerations are given by

$${}'\ddot{u} = H_N{}'\ddot{D}_{Ni} \tag{8}$$

Then substitute Eqs. (1), (3), and (8) into Eq. (6) to obtain for an arbitrary virtual displacement δD_{Mi} the following discretized equation of motion for the ith force component at the Nth node:

$$M_{MNij}{}'\ddot{D}_{Mj} + {}'R_{Ni} = {}'F_{Ni} \tag{9a}$$

where the mass matrix is

$$M_{MNij} = \delta_{ij}\rho h\iint H_N H_M\sqrt{A}\,dx_1\,dx_2 \tag{9b}$$

the internal restoring force is

$${}'R_{Ni} = \frac{1}{2}\iint {}'n^{\alpha\beta}(H_{M,\alpha}H_{N,\beta} + H_{N,\alpha}H_{M,\beta})\sqrt{A}\,dx_1\,dx_2 \times ({}'Y_{Mi} + {}'D_{Mi}) \tag{9c}$$

and the external force is

$${}'F_{Ni} = \iint {}'p_i H_N\sqrt{A}\,dx_1\,dx_2 \tag{9d}$$

Note that $\sqrt{A}$ in Eqs. (9) can be obtained from Eq. (2b) in terms of derivatives of the shape functions and the nodal coordinates, thus, further complicating the integration required to form the element matrices.

Equations (9) represent a set of ordinary differential equations of dynamic equilibrium at time t of every degree of freedom on $'C$. Equations (9) are nonlinear in that 1) material nonlinearities are possible in the restoring force $'R_{Ni}$ because $'n^{\alpha\beta}$ can be replaced by any constitutive equation; 2) $'R_{Ni}$ is nonlinear even if the constitutive equation is linear because $'R_{Ni}$ includes finite displacement components $'D_{Mi}$; and 3) nonconservative loads are possible in the external force $'F_{Ni}$ if the magnitude or direction of $'p_i$ is dependent on displacements, for example, pressure.

In pressurized membranes, nonconservative loads occur during large displacements. The tractions $'p_i$ due to net pressure p normal to the membrane surface $'C$ are

$${}'p_i = \sqrt{{}'A/A}\,p({}'\hat{N}\cdot\hat{e}_i) \tag{10}$$

where the dot between $'\hat{N}$ and $\hat{e}_i$ represents the inner vector product of the unit normal to the surface with the Cartesian base vector $\hat{e}_i$. Because $'\hat{N}$ is defined in terms of the cross product of the deformed base vectors, we replace $'y_i = y_i + {}'u_i$ by Eqs. (1) and find that for pressure loading Eq. (9d) becomes

$${}'F_{Ni} = pe_{kji}\left(\iint H_N H_{Q,1}H_{M,2}\,dx_1\,dx_2\right) \times ({}'Y_{Qk}{}'Y_{Mi} + {}'Y_{Qk}{}'D_{Mj} + {}'Y_{Qk}{}'D_{Mj} + {}'D_{Qk}{}'D_{Mj}) \tag{11}$$

where e_{kji} is the permutation symbol introduced because of the cross product. We see that $'p_i$ and, hence, $'F_{Ni}$ are indeed nonlinear in the displacement components $'D_{Mi}$.

To evaluate the matrices in Eqs. (9), we must integrate products of the shape functions $H_M(x_\alpha)$ and their derivatives over the area of each element. Because of the complexities of the those products, the integrations must be done numerically.[21] Gaussian quadrature can be used for the quadrilateral elements, and Gauss–Hammer formulas can be used for the triangular elements.

C. Nonlinear Forced Vibrations

Here we will develop a solution scheme for predicting the nonlinear dynamic motions. The scheme is a combined incremental and iterative method. We adopt a total Lagrangian approach[19] in which we disregard nonlinear interactions of the membrane with the embedding medium. If we consider the surface ${}^{\#}C$ at a slightly later time $t + \Delta t$ from the surface $'C$ at time t when we assume all variables are known, we can rewrite Eq. (9) at time $t + \Delta t$ as

$$[M]\{{}^{\#}\ddot{D}\} + \{{}^{\#}R\} = \{{}^{\#}F\} \tag{12}$$

where a bracketed term, for example, $[M]$, denotes a matrix, for example, M_{MNij}, and braces about a term, for example, $\{{}^{\#}R\}$, denotes a vector, for example, ${}^{\#}R_{Ni}$. The vectors $\{{}^{\#}R\}$ and $\{{}^{\#}F\}$ are obtainable from Eqs. (9) by replacing the superscript $'$ by ${}^{\#}$. Note that $[M]$ is neither dependent on time nor on displacements and, therefore, needs to be calculated only once.

If we assume that the exact value of $\{{}^{\#}D\}$ at time $t + \Delta t$ is given by an iteration on a prior estimate $\{{}^{\#}\tilde{D}\}$ to the solution, that is,

$$\{{}^{\#}D\} = \{{}^{\#}\tilde{D}\} + \{{}^{\#}\Delta D\} \tag{13a}$$

then we can take Taylor expansions in Eqs. (12) about the solution $\{{}^{\#}\tilde{D}\}$ and obtain a Newton–Raphson iterative equation[22]

$$[M]\{{}^{\#}\ddot{D}\} + [{}^{\#}K]\{{}^{\#}\Delta D\} = (\{{}^{\#}\tilde{F}\} - \{{}^{\#}\tilde{R}\}] \tag{13b}$$

in which $\{{}^{\#}\tilde{F}\} - \{{}^{\#}\tilde{R}\}$ is evaluated at $\{{}^{\#}\tilde{D}\}$ and $[{}^{\#}\tilde{K}]$ is the tangent stiffness matrix evaluated at $\{{}^{\#}\tilde{D}\}$

$$[{}^{\#}\tilde{K}] = \frac{\partial(\{{}^{\#}\tilde{R}\} - \{{}^{\#}\tilde{F}\})}{\partial\{{}^{\#}\tilde{D}\}} \tag{13c}$$

If conservative loads are considered, $\partial\{{}^{\#}\tilde{F}\}/\partial\{{}^{\#}\tilde{D}\} = 0$. If nonconservative loads, such as pressure, are considered, $\{{}^{\#}\tilde{F}\}$ is obtained from Eq. (11) and, therefore,

$$\frac{\partial\{{}^{\#}\tilde{F}\}}{\partial\{{}^{\#}\tilde{D}\}} = pe_{kji}\left[(Y_{Qk} + {}^{\#}D_{Qk})\iint H_N H_{Q,1}H_{M,2}\,dx_1\,dx_2 + (Y_{Qk} - {}^{\#}D_{Qk})\iint H_N H_{M,1}H_{Q,2}\,dx_1\,dx_2\right] \tag{14a}$$

Because of the permutation symbol e_{kji}, we see that Eq. (14a) will contribute nonsymmetric terms to the tangent stiffness matrix. It is often convenient to achieve a symmetric stiffness matrix and, therefore, in one solver described in Sec. IV, the nonsymmetric terms in Eq. (14a) were disregarded, and instead the load $\{{}^{\#}F\}$ in Eq. (12) was treated iteratively to partially account for that nonlinear effect. The full nonsymmetric terms are included in another solver described in Sec. IV.

Thus, the principal term in the tangent stiffness matrix is

$$[{}^{\#}\tilde{K}] = \frac{\partial\{{}^{\#}R\}}{\partial\{{}^{\#}\tilde{D}\}} \tag{14b}$$

and is obtained by taking the indicated derivatives of Eq. (14b),

$$\tilde{K}_{MNij} = \iint\left\{\frac{1}{2}\delta_{ij}{}^{\#}n^{\alpha\beta}(H_{M,\alpha}H_{N,\beta} + H_{N,\alpha}H_{M,\beta}) + \frac{1}{4}C^{\alpha\beta\eta\xi}(H_{R,\alpha}H_{N,\beta} + H_{N,\alpha}H_{R,\beta})(Y_{Ri} + {}^{\#}\tilde{D}_{Ri})(H_{Q,\eta}H_{M,\xi} + H_{M,\eta}H_{Q,\xi})(Y_{Qj} + {}^{\#}\tilde{D}_{Qj})\right\}\sqrt{A}\,dx_1\,dx_2 \tag{15}$$

D. Newmark's Method[19]

Given the solution on $'C$ at time t and the linearized iterative form of the equations of motion, Eqs. (13–15), we seek an incremental solution for the iteration $\{{}^{\#}\Delta D\}$ to the solution on ${}^{\#}C$, Toward that

end, we assume distributions for the velocities $\{{}^{t}\dot{D}\}$ and accelerations $\{{}^{t}\ddot{D}\}$ during the time interval from t to $t+\Delta t$ such that

$$\{{}^{t}\dot{D}\} = \{{}^{\prime}\dot{D}\} + [(1-\alpha)\{{}^{\prime}\ddot{D}\} + \alpha\{{}^{t}\ddot{D}\}]\Delta t \tag{16a}$$

$$\{{}^{t}D\} = \{{}^{\prime}D\} + \{{}^{\prime}\dot{D}\}\Delta t + \left[\left(\tfrac{1}{2}-\beta\right)\{{}^{\prime}\ddot{D}\} + \beta\{{}^{t}\ddot{D}\}\right]\Delta t^2 \tag{16b}$$

where α and β are parameters dictating the assumed distribution of acceleration over the interval; different explicit and implicit formulations can be developed with different parameters. If α is equal to or greater than 0.5 and if β is equal to or greater than $0.25(0.5+\alpha)^2$, the formulation is implicit.[19]

In the implicit formulation Eq. (16b) is solved for $\{{}^{t}\ddot{D}\}$ in terms of values at time t and in terms of $\{{}^{t}D\}$. On substitution into Eqs. (13), an equivalent static problem is derived at each time step in the form

$$[K_{\text{eff}}]\{{}^{t}\Delta D\} = \{\bar{F}\} - \{R_{\text{eff}}\} \tag{17a}$$

where

$$[K_{\text{eff}}] = [{}^{t}K] + [M]/(\beta\Delta t^2) \tag{17b}$$

is the effective stiffness matrix and $\{\bar{F}\} - \{R_{\text{eff}}\}$ is the similarly modified load vector.

E. Damping

Artificial damping of results, particularly of higher modes of vibration, can be realized by varying the Newmark parameter α in Eqs. (16). If $\alpha = 0.5$, no artificial damping is introduced. For increasingly larger values of α beyond 0.5, increasingly rapid artificial damping is achieved. This would be desired if steady-state, rather than transient, solutions are sought.

If real damping is present in the system, or an alternative artificial damping mechanism is sought, Rayleigh damping proportional to the stiffness and mass matrices can be introduced. Add a damping term $[{}^{t}C]\{{}^{t}\dot{D}\}$ to Eq. (15) with the damping matrix assumed to have the form[23]

$$[{}^{t}C] = \eta[M] + \lambda[{}^{t}K] \tag{18a}$$

and then add appropriate terms to $[K_{\text{eff}}]$ and $\{R_{\text{eff}}\}$. For larger values of η, the lower transient modes are more heavily damped. For larger values of λ, the higher transient modes are more heavily damped. The damping ratio ξ relative to critical damping of a particular modal frequency ω is given in terms of η and λ by[19]

$$\xi = \eta/(2\omega) + \lambda\omega/2 \tag{18b}$$

IV. Computer Implementation

The SD theory described in the preceding section has been implemented in a general purpose FORTRAN computer code, called TENSION, for analysis of the nonlinear dynamic response of cable and membrane structures. Numerous special features have been added to this code to facilitate computer simulation of parachute dynamics. A custom pre- and postprocessor written in MATLAB® has also been developed to provide for state-of-the-art model generation and visualization of the simulation results.

TENSION currently has three dynamic solvers. Two implicit solvers are based on Newmark's method, and the third is based on the explicit central difference method,[19] which is a conditionally stable method. The difference between the two implicit solvers is in the method used to solve the algebraic equations given by Eq. (17a). The first uses a direct factorization method[21] with a profile reduction algorithm[24] and is only applicable to symmetric systems, and the second employs an iterative method[25,26] that can be used for nonsymmetric systems of equations.

V. Results

In this section, three example problems are presented to demonstrate the capabilities of TENSION for simulating parachute dynamics. All three problems are performed as standalone SD simulations. The fluid effects are approximated by prescribing representative pressures on the canopy membranes and by including velocity dependent fluid drag forces on cables and concentrated masses.[8] All examples utilize a linear elastic material model with constant material properties. The properties used in these simulations are $E = 4.32 \times 10^6$ lb/ft^2 $= 0.207$ GPa, $\nu = 0.3$, membrane thickness $= 0.03$ mm (0.0001 ft), cable cross-sectional area $=$ 9.29 mm^2 (0.0001 ft^2), fabric density $= 309.3$ kg/m^3 (0.6 slugs/ft^3), air density $= 1.222$ kg/m^3 (0.00237 slugs/ft^3), and gravitational acceleration $= 9.81$ m/s^2 (32.2 ft/s^2).

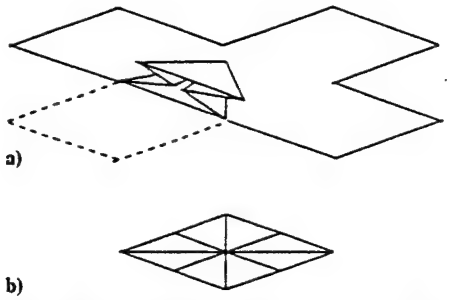

Fig. 1 Initial folded configuration of cross canopy, a) folding of one arm (upside down) and b) entire canopy.

A. Opening and Control of a Cross-Type Canopy

This example demonstrates the ability of TENSION to simulate the opening of a full three-dimensional unconstrained model of a cross-type parachute in an initially folded configuration and subsequent control of the parachute motion through user-defined changes of the control line lengths. The four arms of the cross canopy are initially folded over the canopy center, as shown for one arm in Fig. 1. In this simulation, the model is subjected to constant canopy pressure, cable and payload drag that is dependent on the square of the relative velocity, and gravity. Time-dependent mass proportional damping is applied during the initial opening to stabilize the simulation, then reduced after partial opening is achieved. The initial geometry and deformed geometries at three times during opening are shown in Fig. 2.

Following the opening, the model approaches a steady-state descent. Next, four separate control line length changes are prescribed to simulate the parachute flying in a box pattern. Control line changes are effected in the FEM model by prescribing time-dependent unstressed cable lengths. Each control operation consists of lengthening a control line for 10 s, then retracting it for 10 s prior to initiating the next control operation. The x, y, and z velocities of the payload for the entire simulation are shown in Fig. 3. Prior to control, the horizontal (x, y) velocities are zero, and terminal velocity is approached in the vertical z direction. Control operations begin at 20 s and induce the horizontal velocities shown. The trajectory of the payload is shown in Fig. 4. Here, the initial descent prior to control and the four periods of control are clearly evident. The deformed shape of the parachute model initiating the first control operation is shown in Fig. 5.

B. Opening of a Ram-Air Parafoil System

This model simulates a ram-air parafoil (wing) that is similar to that flown under the U.S. Army GPADS[27] and NASA X-38[28] programs. For simplicity and reduction of computational time, the parafoil is modeled in half-plane symmetry. The wing is initially in a flat configuration that represents the cut pattern geometry. Figure 6 shows the full three-dimensional initial geometry.

The pressure distribution used in this simulation is constant for all time. This is possible due to time-dependent mass proportional damping that is slowly minimized during the early portion of the simulation. The top, bottom, and side faces are supplied different pressure distributions. The system is acted on by a gravitational load in the negative z direction, mass proportional damping, and velocity-dependent cable drag.

The time-dependent mass proportional damping is ramped from an initially high value to a low value over the first 5 s of the simulation. These values allow for a slow oozing of the parafoil into the inflated shape and a method of allowing the suspension lines, all of which start in a slack state, to become axially loaded. The program allows the user to define the cable length between two nodes to be longer than the actual distance between the nodes and to prescribe

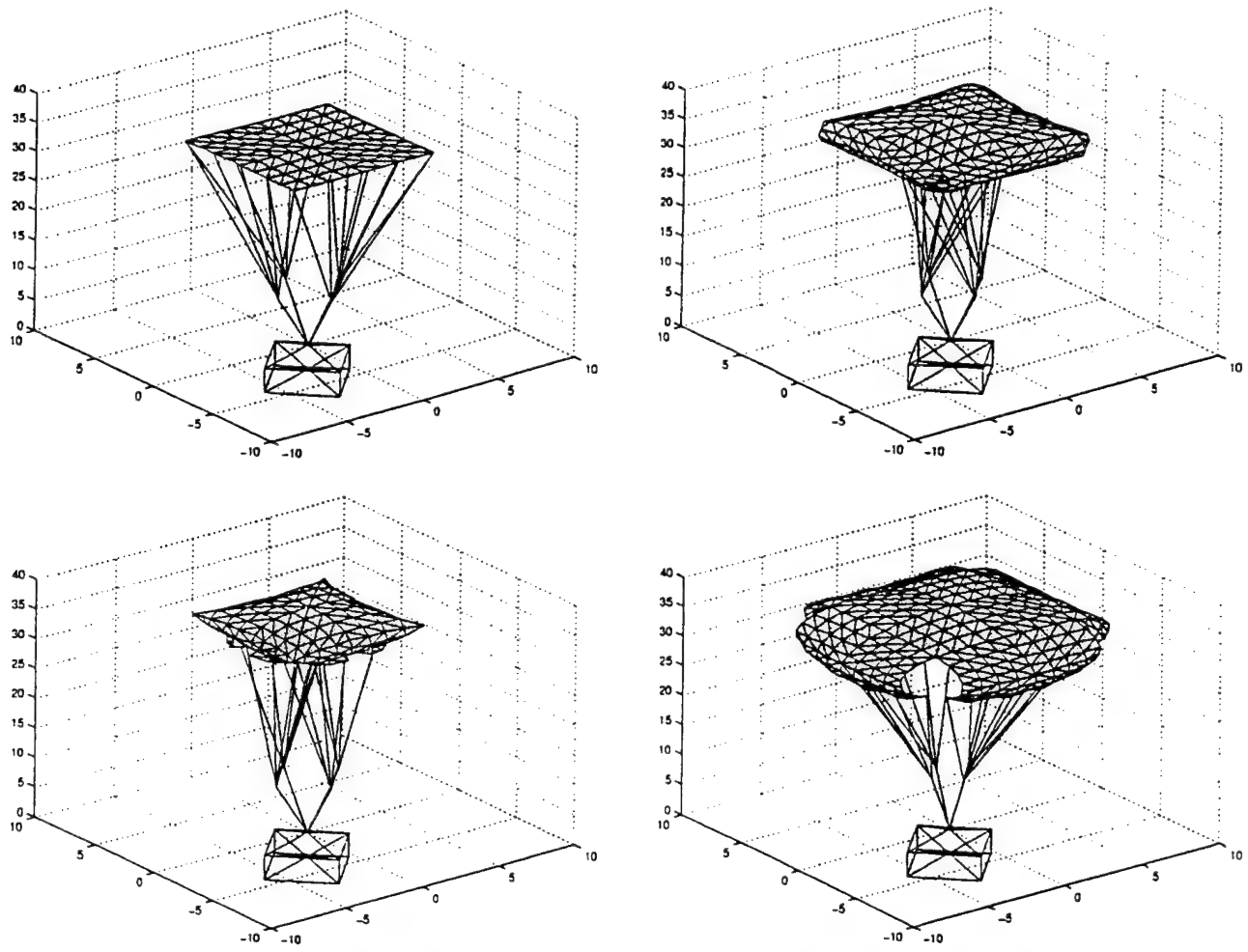

Fig. 2 Initial configuration and deformed shapes during initial opening of cross parachute.

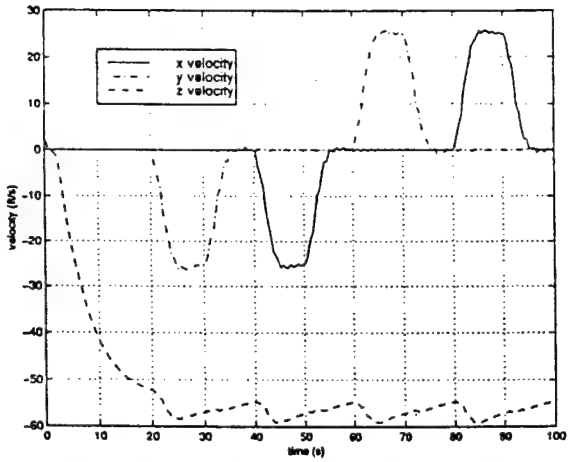

Fig. 3 Payload velocity of cross parachute.

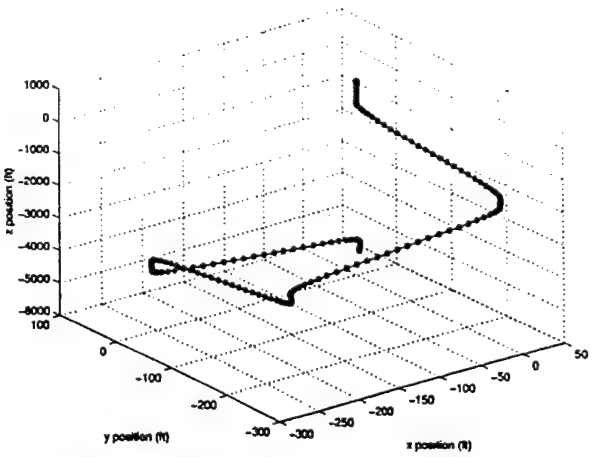

Fig. 4 Trajectory of payload of cross parachute.

that the cable is in a slack state. This is a critical capability that allows the user to run the same model (same nodal coordinates) with different sets of suspension line and bridle lengths. The user can also prescribe changes in cable lengths in time that could be used to predict the effect on the systems performance to changes in rigging angle. As already mentioned, all suspension lines are initially in a slack state with a user-defined cut length. This also assists in model development due to the relatively simple geometry and the ability to incorporate actual cut patterns for the canopy. The time-dependent mass proportional damping allows for the smooth transition to an inflated shape and transition into steady-state glide. Figure 7 shows a sequence of snapshots during the initial inflation process.

The system slowly reaches a steady-state glide after approximately 40 s. Figure 8 shows the y and z positions of the payload and node A vs time. At a simulation time of 45 s, six trailing-edge control lines are shortened to a predefined length over a 5-s time interval to simulate a flare manuver. The pressure loading on the system during a flare will most definitely change over time; however, for this simulation, the pressure is assumed constant. The y and z velocities of the payload and node A are shown in Fig. 9, which clearly shows the effect of the flare maneuver.

This example demonstrates the ability of TENSION to simulate the inflation of a parafoil starting from cut patterns to a steady-state glide with the potential of the user modifying the rigging angle in

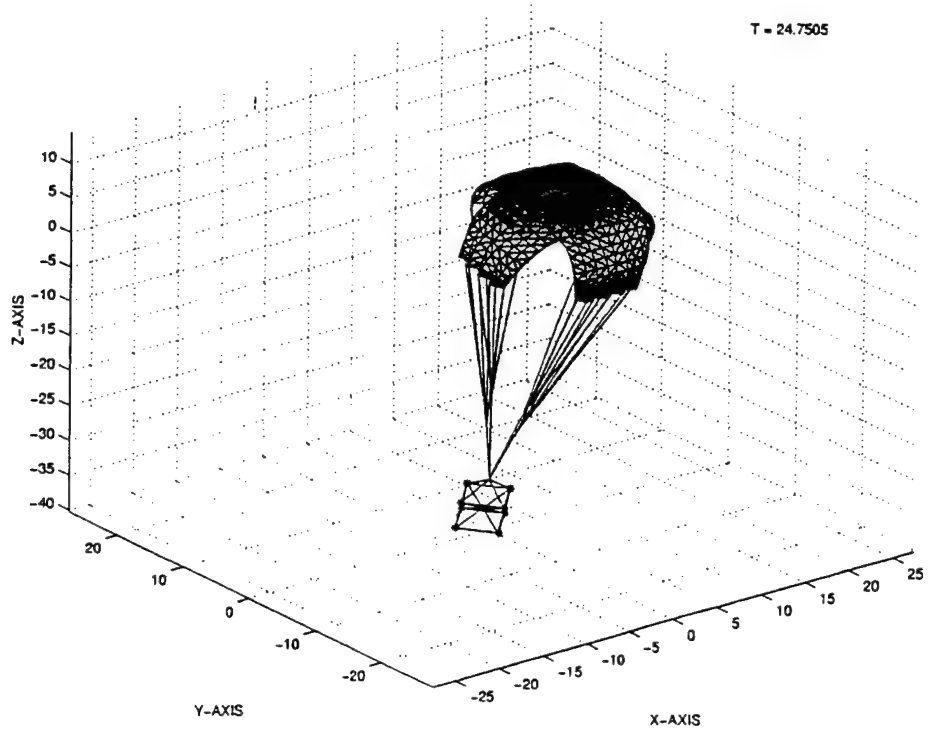

Fig. 5 Deformed shape of cross parachute during first control operation.

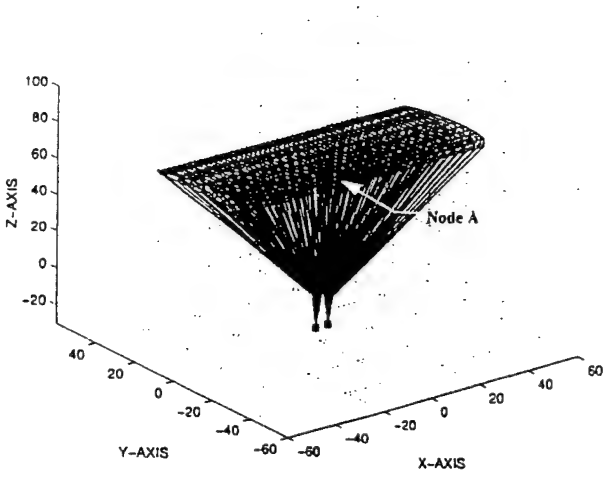

Fig. 6 Initial geometry of parafoil model.

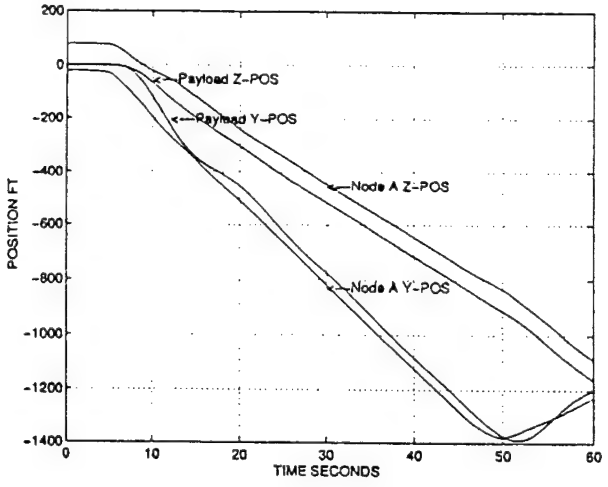

Fig. 8 Position vs time curves for parafoil simulation.

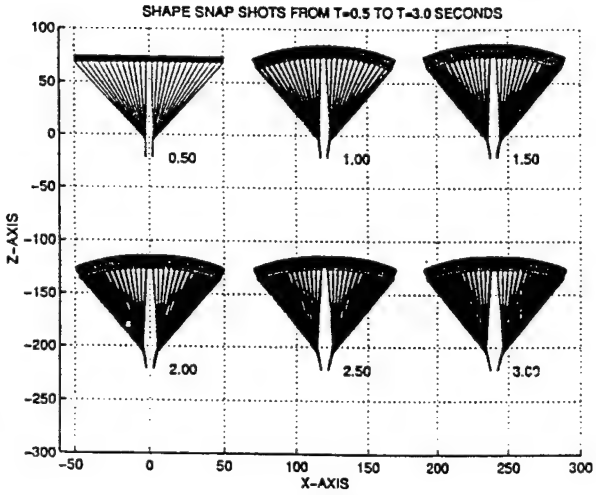

Fig. 7 Deformed shapes during parafoil inflation.

time to optimize design and a flare-type control maneuver. Generalization to a fully three-dimensional unconstrained model for turn performance predictions is expected to be a small modification that would simply increase the overall model size.

C. Opening of a Round Canopy

The third example is a generic round ring-slot canopy. The model consists of 28 gores and 6 ring slots. The model starts in a folded configuration, as shown in Fig. 10. The simulation begins with an initial horizontal velocity on all node points in the negative x direction. Note that all 28 gores are folded along the gore centerlines in a configuration that is close to that obtained at line stretch. The model is fully three-dimensional and unconstrained. The model is subjected to a vertical gravitational loading, user-defined time-dependent pressure distribution, velocity-dependent cable drag, and velocity-dependent payload drag. Time-dependent mass proportional damping is minimally present over the first 4 s of the simulation.

A time-dependent outward acting pressure distribution is simultaneously applied to all membrane elements. Gravity is acting throughout the simulation. The seam cables, suspension line cables,

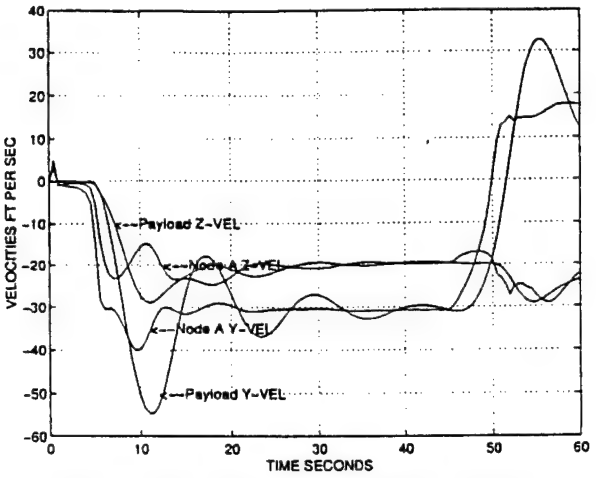

Fig. 9 Velocity vs time curves for parafoil simulation.

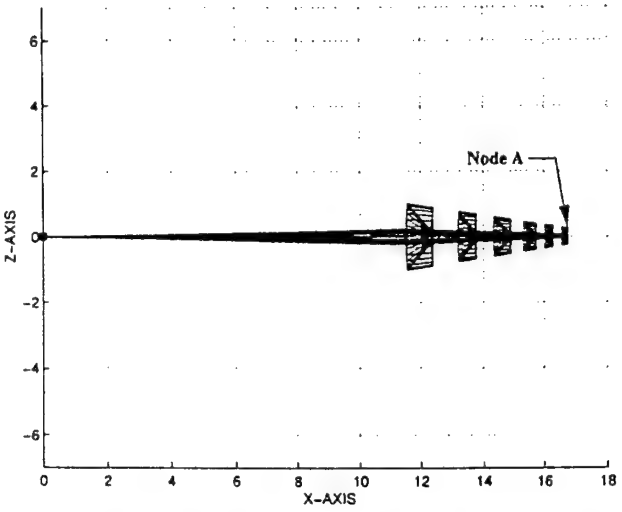

Fig. 10 Initial folded configuration of ring-slot parachute.

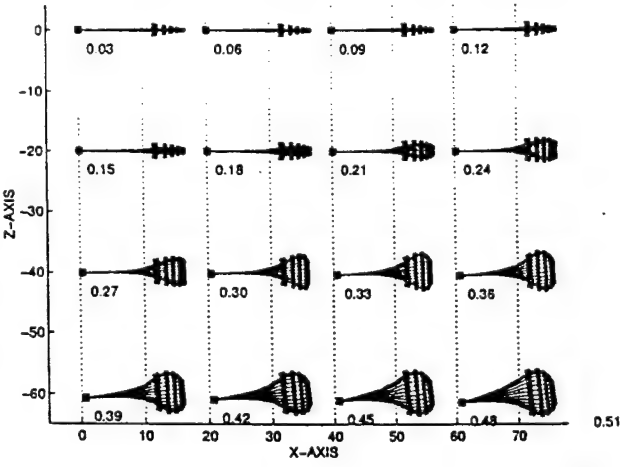

Fig. 11 Deformed shapes of ring-slot parachute during inflation (0.03–0.48 s).

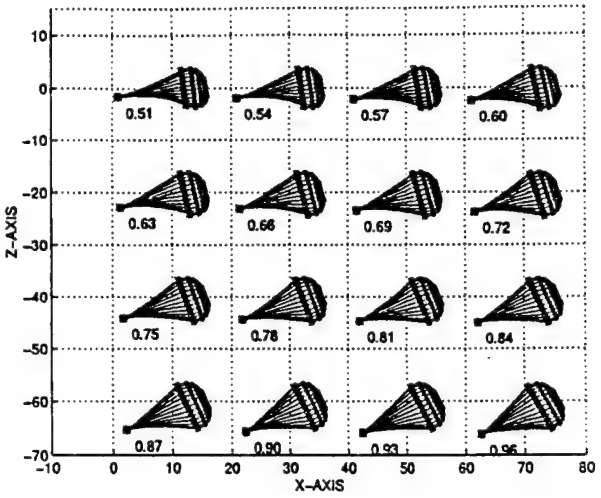

Fig. 12 Deformed shapes of ring-slot parachute during inflation (0.51–0.96 s).

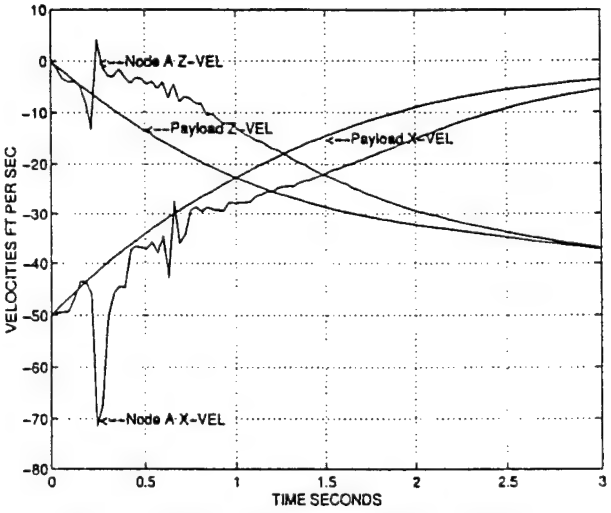

Fig. 13 Velocity vs time curves for ring-slot parachute.

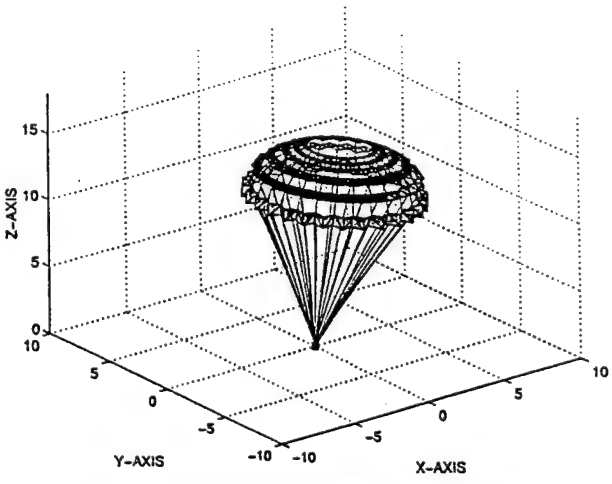

Fig. 14 Final shape of ring-slot parachute.

and payload are subjected to velocity-dependent drag loads for all times, which assists in the trajectory changing from pure horizontal motion to pure vertical motion.

A sequence of payload-fixed snapshots are shown in Figs. 11 and 12 for time intervals of 0.03–0.48 and 0.51–0.96 s, respectively. These snapshots clearly show the three-dimensional capabilities of TENSION. For example, the uppermost suspension lines become stressed and elongated during the inflation before the lowermost suspension lines. The lower suspension lines also appear to be most visibly affected by the fluid drag. Figure 13 shows the horizontal and vertical velocities of the payload and node A vs time. The system's final shape is shown in Fig. 14.

This model demonstrates the ability of TENSION to simulate a round canopy with an initial horizontal velocity and folded configuration through opening and ultimately into a steady-state vertical terminal configuration.

VI. Conclusions

The finite element formulation for an SD model capable of simulating the nonlinear dynamic behavior of highly flexible structures comprising membranes and cables has been presented. This model is currently being used to simulate the inflation, terminal descent, and control of a variety of parachute systems. Three example problems were presented to demonstrate the capabilities of this model for simulating parachute dynamics. In these examples, the effect of the surrounding airflow was approximated by prescribing the membrane pressure and cable and payload drag on the structural model. Coupling of the structural model with CFD programs has been presented in other publications.[14,15] The ultimate goal of these efforts is to be able to design and optimize parachute systems using computer simulations, reduce the life cycle costs of airdrop systems, and provide an airdrop virtual proving ground.

Acknowledgments

This material is based on work supported in part by the U.S. Army Research Office under Grant DAA04-96-1-0051 and in part by the U.S. Air Force Office of Scientific Research under Grant F49620-98-1-0214 to the University of Connecticut.

References

[1]Strickland, J. H., and Higuchi, H., "Parachute Aerodynamics: An Assessment of Prediction Capability (1995)," AIAA Paper 95-1531, May 1995.

[2]Knacke, T. W., "Parachute Recovery Systems Design Manual," *NWC TP 6575*, Naval Weapons Center, China Lake, CA, June 1987.

[3]Purvis, J. W., "Improved Prediction of Parachute Line Sail During Lines-First Deployment," AIAA Paper 84-0786, April 1984.

[4]Sundberg, W. D., "Finite-Element Modeling of Parachute Deployment and Inflation," AIAA Paper 75-1380, Nov. 1975.

[5]Haug, E., Lasry, D., and de Kermel, P., "Dynamic Simulation of Industrial Membranes Including Their Interaction with Surrounding Media," *Third International Symposium of the SFB 230 "Evolution of Natural Structures,"* Univ. of Stuttgart, Germany, Oct. 1994.

[6]Stein, K., Benney, R., Kalro, V., Johnson, A., and Tezduyar, T., "Parallel Computation of Parachute Fluid–Structure Interactions," AIAA Paper 97-1505, June 1997.

[7]Mosseev, Y., "The Multipurpose Integrated PC Software for Structural and Aeroelastic Analysis of Decelerators, Paragliders, and Balloons," AIAA Paper 97-1455, June 1997.

[8]Benney, R., Stein, K., Leonard, J., and Accorsi, M., "Current Three-Dimensional Structural Dynamic Finite Element Modeling Capabilities," AIAA Paper 97-1506, June 1997.

[9]Chuzet, L., "Numerical Determination of Parachutes Performances with SINPA Software," AIAA Paper 97-1509, June 1997.

[10]Sahu, J., and Benney, R., "Prediction of Terminal Descent Characteristics of Parachute Clusters Using CFD," AIAA Paper 97-1453, June 1997.

[11]Kalro, V., Gerrard, W., and Tezduyar, T., "Parallel Finite Element Simulation of the Flare Maneuver of Large Ram-Air Parachutes," AIAA Paper 97-1506, June 1997.

[12]Lacroix, C., Ibos, C., Chuzet, L., and Granville, D., "SINPA-A Full Three-Dimensional Fluid–Structure Software for Parachute Simulation," AIAA Paper 97-1508, June 1997.

[13]Nelsen, J. M., "Computational Fluid Dynamics Studies of a Solid and Ribbon 12-Gore Parachute Canopy in Subsonic and Supersonic Flow," AIAA Paper 95-1558, May 1995.

[14]Stein, K., Benney, R., Kalro, V., Tezduyar, T., Leonard, J., and Accorsi, M., "Parachute Fluid–Structure Interactions: 3-D Computation," *Computer Methods in Applied Mechanics and Engineering* (to be published).

[15]Benney, R., Stein, K., Kalro, V., Tezduyar, T., Leonard, J., and Accorsi, M., "Parachute Performance Simulations: A 3D Fluid–Structure Interaction Model," 21st Army Science Conf., Norfolk, VA, June 1998.

[16]Stein, K., Benney, R., Kalro, V., Tezduyar, T., Bretl, T., and Potvin, J., "Fluid–Structure Interaction Simulations of a Cross Parachute: Comparison of Numerical Predictions with Wind Tunnel Data," AIAA Paper 99-1725, June 1999.

[17]Leonard, J. W., *Tension Structures*, McGraw–Hill, London, 1988.

[18]Lo, A., "Nonlinear Dynamic Analysis of Cable and Membrane Structures," Thesis Oregon State Univ., Corvallis, OR, June 1982 (submitted).

[19]Bathe, K. J., *Finite Element Procedures*, Prentice–Hall, Upper Saddle River, NJ, 1996.

[20]Green, A. E., and Adkins, J. E., *Large Elastic Deformations and Nonlinear Continuum Mechanics*, Oxford Univ. Press, Oxford, England, UK, 1960, 2nd ed., 1970.

[21]Atkinson, K. E., *An Introduction to Numerical Analysis*, 2nd ed., Wiley, New York, 1989.

[22]Oden, J. T., *Finite Elements of Nonlinear Continua*, McGraw–Hill, New York, 1972.

[23]Clough, R. W., and Penzien, J., *Dynamics of Structures*, McGraw–Hill, New York, 1975.

[24]Sloan, S. W., "A FORTRAN Program for Profile and Wavefront Reduction," *International Journal for Numerical Methods in Engineering*, Vol. 28, 1989, pp. 2651–2679.

[25]Saad, Y., and Schultz, M., "GMRES: A Generalized Minimal Residual Algorithm for Solving Nonsymmetric Linear Systems," *SIAM Journal on Scientific and Statistical Computing*, No. 7, 1986, pp. 856–869.

[26]Kennedy, J. G., Behr, M., Kalro, V., and Tezduyar, T., "Implementation of Implicit Finite Element Methods for Incompressible Flows on the CM-5," *Computer Methods in Applied Mechanics and Engineering*, Vol. 119, 1994, pp. 95–111.

[27]Wailes, W., and Harrington, N., "The Guided Parafoil Airborne Delivery System Program," AIAA Paper 95-1538, May 1995.

[28]Wilson, J. R., "CRV Investment Offers Safe Return," *Aerospace America*, June 1997, pp. 28–32.

S. Saigal
Associate Editor

AIAA 2000-4310
Fluid-Structure Interaction Modeling of the US Army Personnel Parachute System

Richard J. Benney and Keith R. Stein
US Army Soldier Systems Center
Natick, MA

Tayfun E. Tezduyar
Rice University
Houston, TX

Michael L. Accorsi, Wenqing Zhang, and John W. Leonard
University of Connecticut
Storrs, CT

AIAA Guidance, Navigation and Control Conference & Exhibit

14-17 August 2000
Denver, Colorado

FLUID-STRUCTURE INTERACTION MODELING OF THE US ARMY PERSONNEL PARACHUTE SYSTEM †

Richard J. Benney, Keith R. Stein,
U.S. Army Soldier and Biological Chemical Command
Soldier Systems Center - Natick, MA 01760
Richard.Benney@natick.army.mil, Keith.Stein@natick.army.mil,

Tayfun E. Tezduyar
Mechanical Engineering and Materials Science
Rice University, TX 77005
tezduyar@rice.edu,

Michael L. Accorsi, Wenqing Zhang, and John W. Leonard
Department of Civil and Environmental Engineering
University of Connecticut, CT 06269
accorsi@engr.uconn.edu, wenqingz@engr.uconn.edu, leonard@engr.uconn.edu

ABSTRACT

We present a strategy for carrying out 3–D simulations of parachute fluid–structure interaction, and demonstrate the strategy for simulations of airdrop performance and control phenomena in terminal descent. The strategy uses a stabilized space–time formulation of the time–dependent, 3–D Navier–Stokes equations of incompressible flows for the fluid dynamics solution. A finite element formulation derived from the principle of virtual work is used for the parachute structural dynamics. Coupling of the fluid dynamics with the structural dynamics is implemented over the the fluid–structure interface, which is the parachute canopy surface. Large deformations of the structure are handled in the fluid dynamics mesh using an automatic mesh moving scheme. The strategy is demonstrated to simulate the terminal descent behavior of a standard US Army personnel parachute system. Also, preliminary simulations are presented for the response of the parachute to a variety of "riser slips," which can provide the parachute system with limited maneuverability.

INTRODUCTION

Airdrop technology is a vital Department of Defense (DoD) capability to the rapid deployment of warfighters, ammunition, equipment and supplies. In addition, airdrop of food, medical supplies, and shelters for humanitarian relief efforts are increasing in demand. A team of researchers centered at the US Army Soldier and Biological Chemical Command (SBCCOM), Natick Soldier Center (Natick) are actively involved in developing new technologies to advance DoD airdrop capabilities. An important technology being developed is the numerical modeling of parachutes and airdrop system performance utilizing high performance computing (HPC) resources. Parachutes and airdrop systems have been traditionally developed by time consuming and costly full-scale testing. The capability of using HPC tools to model and develop parachutes and airdrop systems will greatly reduce the time and cost of full-scale testing, help to minimize the life cycle costs of airdrop systems, assist in the optimization of new airdrop capabilities, and provide an airdrop virtual proving ground environment.

These modeling efforts generally involve the coupling of computational fluid dynamics (CFD) codes and structural dynamics (SD) codes. These coupled fluid-structure interaction (FSI) models are required to capture the physics of highly complex parachute dynamic phenomena. Applications and focus areas include most airdrop systems and associated phenomena. This paper will focus on the US Army's mass assault personnel parachute in terminal descent and with riser control inputs. The T–10 parachute system consists of a flat extended skirt canopy, 30 suspension lines and four 3-foot risers attaching to the paratroopers harness. A detailed description of the structural model of the canopy

and the associated fluid model for the surrounding airfield will be presented.

Paratroopers are trained at the basic airborne school at Fort Benning, Georgia. The three week course includes training in controlling a T–10 parachute (the current mass assault parachute for US Army troops) by use of riser slips. Riser slips involve physically reaching up and grabbing a riser and pulling it down to modify the canopy shape and induce glide. Riser slips are used to avoid close contact with other jumpers, avoid ground obstacles, and to "pull a two riser slip into the wind" and hold it approximately 150 to 200 feet above the ground to minimize relative horizontal ground impact speeds. Experienced paratroops can control the T–10 that is typically a non-controllable round parachute.

Riser slips are used routinely every day but are not fully understood. The effects of riser slip length, jumper weight, and other variables on the relative horizontal velocity of the system are not well known beyond jumpers practical experience. The US Army and US Air Force are exploring the use of riser slips for use in high-altitude resupply cargo systems to allow for precision landing (i.e., target accuracy) for various weight payloads. These are autonomously controlled round parachutes in which the risers are replaced by actuators and which utilize GPS as the primary navigation sensor.[1] These systems require knowledge of achievable performance in order for control optimization strategies to be developed. Currently, the only way to determine the performance characteristics is through extensive instrumented testing of full-scale systems.

In addition, the Army is exploring an Advanced Tactical Parachute System (ATPS) to replace the T–10. The canopy chosen will not use a T–10 and therefore, the systems response to a riser slip will need to be determined and measured for comparisons to the current T–10 to assess potential operational impacts. Once again, this will require extensive testing. The FSI capabilities being developed are being applied to these two real and current applications. Concurrently, and reported in this paper, the prediction of the performance of a T–10 in terminal descent and during a riser slip will be presented as a base line example. A series of detailed measurements of T–10 parachutes with personnel pulling riser slips is being conducted in partnership with the US Army Yuma Proving Ground (the primary testing agency for such systems). However, the data was not available when this paper was written.

The ultimate goal of this work is to utilize these tools to minimize feasibility testing of new systems, assist in determining the capabilities of all systems, and ultimately to reduce the life cycle cost of all DoD Airdrop Systems. This paper will provide an overview of the FSI theory and finite element strategy being developed and provide a status report on the ability to predict T–10 performance in terminal descent and during controlled riser deformations.

MODELING STRATEGY

Fluid Dynamics

For the fluid dynamics, the flow is assumed to be at a low speed and thus the Navier-Stokes equations of incompressible flows are utilized. To handle the time-variant spatial domains encountered in parachute problems, we employ the Deforming–Spatial–Domain/Stabilized Space–Time (DSD/SST) formulation[2,3] finite element formulation. In this formulation, the finite element interpolation polynomials are functions of both space and time, and the stabilized variational formulation of the problem is written over the associated space-time domain. This stabilized formulation automatically takes into account deformations in the spatial domain and protects the computation against numerical oscillations. This method has been applied to a large number of problems with moving boundaries and interfaces.

Structural Dynamics

The parachute structure is represented as a "tension structure" composed of membranes, cables, and point masses. For our problems, the structure undergoes large displacements and large rotations, but small strains. Thus, constitutive relationships are used assuming the materials are Hookean with linear-elastic properties. A finite element formulation derived from the principle of virtual work is used for the structural dynamics (SD).[4,5] Finite displacements of the structure are taken into account by using a total Lagrangian description of the problem. In addition to membrane and cable elements, a variety of parachute-specific features have been incorporated into the SD solver to include wrinkling models[6] (which eliminate compressive stresses) and time-variant cable lengths[7] (for modeling of control line pulls, "riser-slips", reefing, etc.).

Mesh-Moving Strategy

We use an automatic mesh-moving scheme to handle changes in the spatial domain due to

parachute canopy deformations. In this scheme, the fluid mesh is treated as a linearly-elastic "pseudo-solid" that deforms as dictated by the motion of the surface boundaries of the fluid domain.[8] This scheme introduces an additional computational cost associated with the mesh-moving equations, but is well suited for handling the complex geometries and arbitrary motions for this class of problems.

Fluid-Structure Coupling

The fluid-structure coupling occurs at the FSI interface, which is in this case the parachute canopy surface. We use an iterative coupling approach, with individual systems of equations being solved for the fluid and the structure. Coupling is achieved through the transfer of FSI information between the fluid and structure within an iteration loop, with multiple iterations improving the convergence of the coupled system. Displacements and displacement rates from the SD solution are treated as boundary conditions in the mesh moving scheme and CFD solver, respectively. In return, parachute surface tractions from the fluid are used as distributed forces in the SD solver. For the applications presented in this paper, we transfer only the pressure contribution from the CFD solution to the SD solver.

In the example problems, we use different meshes to represent the parachute canopy in the SD and CFD models. Biquadradic elements define the canopy in the SD mesh (to effectively represent curvatures in the membranes), whereas triangular elements define the canopy surface in the CFD mesh (in order to utilize automatic mesh generation software). Coupling information is transferred between the incompatible meshes using a least-squares projection strategy. Figure 1 depicts the incompatible meshes used for the example problems to be presented. Here, the parachute canopy is represented with 9–noded membranes elements in the SD mesh and with 3–noded triangles in the CFD mesh.

T–10 PARACHUTE APPLICATIONS

The described FSI modeling strategy is being demonstrated for a variety of parachute applications to include the the terminal descent of the Army's T–10 personnel parachute system.[9–13] The T–10 is a "flat extended skirt canopy" composed of a 35-foot diameter (D_c) canopy and 30 suspension lines each 29.4 feet long. The canopy is called a "flat extended skirt canopy" because in its constructed (or nonstressed) configuration it is composed of a main

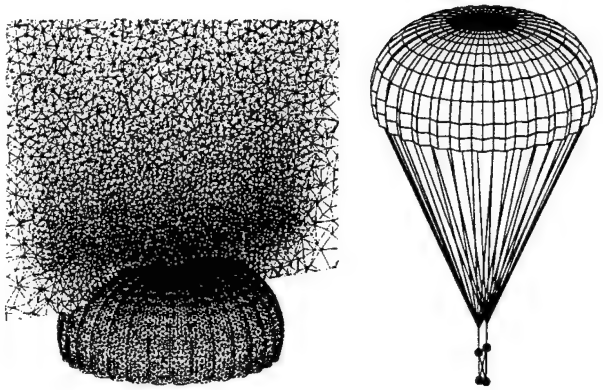

Figure 1. Incompatible meshes for T–10 parachute.

circular section with a circular vent at the apex and an inverted flat ring section, which lies under the main section and is connected to the main section at the outer radius. The lines are connected to the payload (i.e., paratrooper) with four risers. The suspension lines continue as 30 gore-to-gore reinforcements through the parachute canopy and meet at the apex. For the T–10, the vent diameter is $0.1D_c$ and the width of the skirt is also $0.1D_c$. Figure 2 shows a "blown–out" view for the SD mesh.

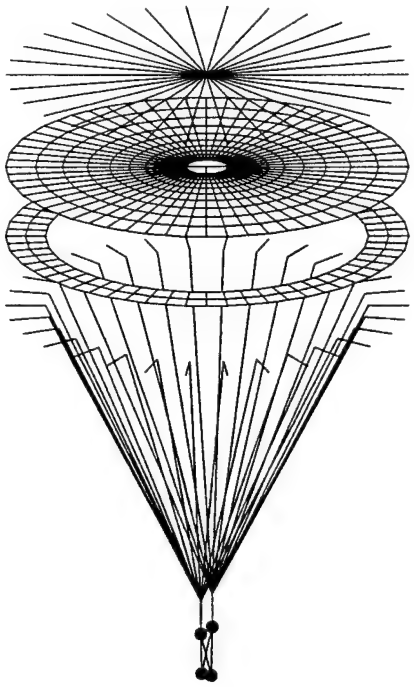

Figure 2. SD mesh for T–10 parachute.

T–10 Parachute in Terminal Descent

The following example is for the FSI of a Army personnel parachute in terminal descent freefall. The simulation process involves three main steps.

Stand-alone structural dynamics simulation:

The SD model is broken into six distinct material groups; one membrane group, three cable groups, a truss group, and a concentrated mass group. The membrane group defines the parachute canopy. We have distinct cable groups for the suspension lines, the canopy radial reinforcements, and the risers. The truss and concentrated mass groups define the payload. The SD mesh consists of 3,593 nodes, 780 nine-noded (i.e., biquadratic) membrane elements for the canopy surface, and 1,196 two-noded cable elements, and 4 concentrated mass points. The parachute system is represented by linearly elastic materials, with properties representative of a T–10. A stand-alone damped dynamic simulation is conducted for the T–10 parachute model to inflate the canopy under a prescribed differential pressure of 0.5 lb/ft^2. For the stand-alone simulation, the four payload node points are fixed in space and all other nodes are unconstrained. The equilibrium shape for the inflated parachute is depicted in Figure 1 (right). This equilibrium solution is used as the initial condition for the SD solver in the subsequent FSI simulation.

Stand-alone fluid dynamics simulation:

A 3-D mesh with tetrahedral elements is generated (with 149,253 nodes and 888,344 elements) using the inflated canopy from the stand-alone SD simulation as an interior boundary. Initial unsteady flow solutions are obtained for the fixed canopy configuration at a Reynolds number of 5×10^6 using a stabilized semi-discrete formulation.[14] For the flow simulations, the parachute canopy is treated as a zero-porosity material and the parachute canopy is assigned a no-slip boundary condition. The inflow boundary below the parachute is assigned a prescribed velocity condition equivalent to the desired Reynolds number. Side boundaries are assigned free-slip conditions, and the outflow boundary above the parachute is assigned a traction-free condition. The semi-discrete formulation, which is less cost-intensive than the DSD/SST formulation, is adequate for the stand-alone simulations since there is no time dependence in the spatial domain (i.e., no deformations of the canopy). After this flow is developed, several time steps were computed, still with the fixed canopy but by using the DSD/SST procedure, to obtain the starting CFD conditions for the FSI simulation. The developed pressure field and velocity field are shown in Figure 3.

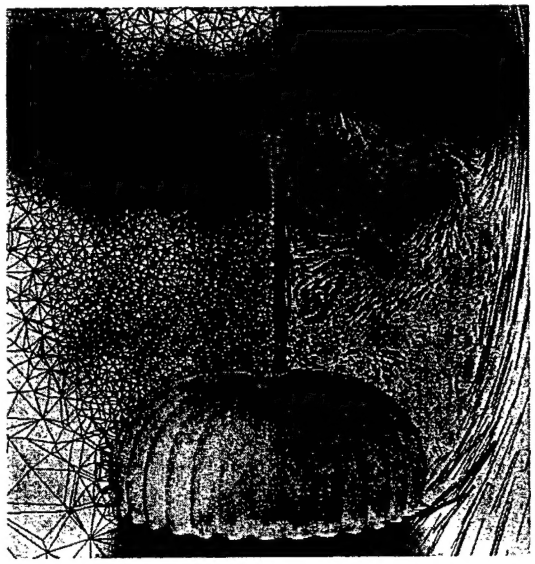

Figure 3. Inflated T–10: Initial CFD mesh and flow-field.

Stand alone FSI simulation:

Final conditions from the stand alone simulations are used to initiate the FSI simulation. Here, the parachute structure is totally unconstrained. To handle the motion of the parachute, the fluid mesh moves globally relative to the mean parachute canopy displacement and the canopy shape changes are accounted for in the CFD mesh using the automatic mesh moving scheme. The deforming parachute, with the canopy differential pressures, for the FSI simulation are shown at four instants in time in Figure 4. Figure 5 shows the computed drag force in comparison to the total gravitational force acting on the parachute system (i.e., canopy, suspension lines, risers, and payload weights). As expected, the drag force oscillates about the weight of the parachute system.

Control Line Pulls

The ability to simulate riser pulls was initially demonstrated for a "soft landing" of a T–10 FSI simulation.[13] Here, a soft-landing was accomplished by smoothly decreasing in time the natural lengths of the cable elements defining each of the four risers. The preliminary soft-landing simulation is being extended to study the response of the parachute system to single- and double-riser pulls and releases.

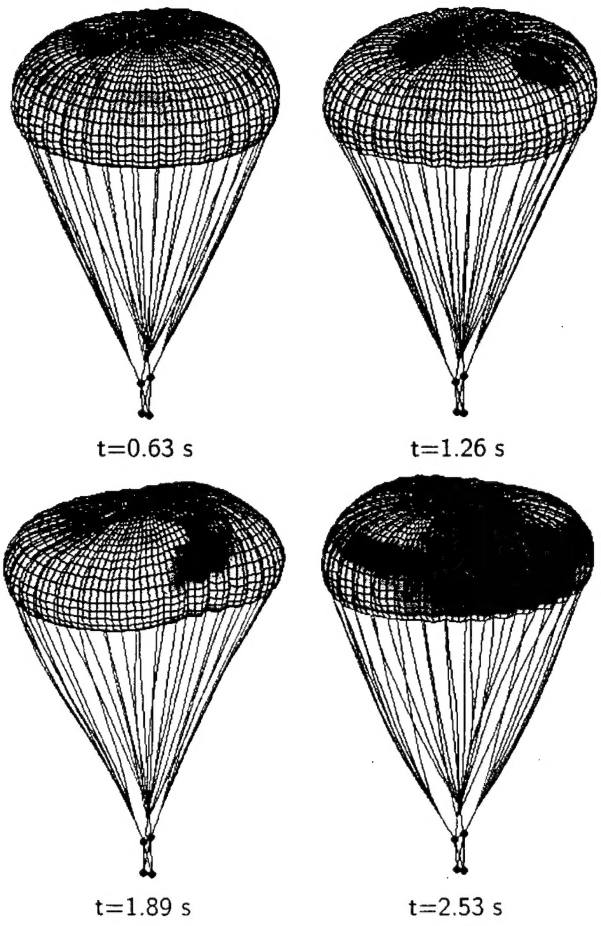

Figure 4. T–10 parachute during FSI simulation (Colored with differential pressure).

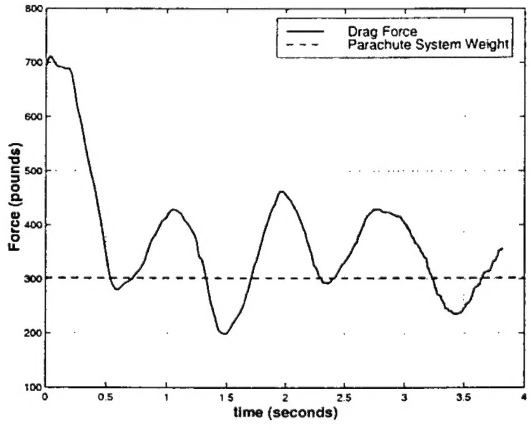

Figure 5. Drag force.

Figure 6 shows the inflated configuration for the T–10 parachute shaded with the maximum principal stresses in the canopy after stand-alone SD simulations for the standard configuration, for single- and double-riser pulls of 2.5 feet, and for single- and double-riser releases of 3.0 feet. Loss of symmetry in the parachute canopy resulting for the riser pulls and releases is evident. These asymmetries provide the canopy with lift which can be used to steer or redirect the parachute system.

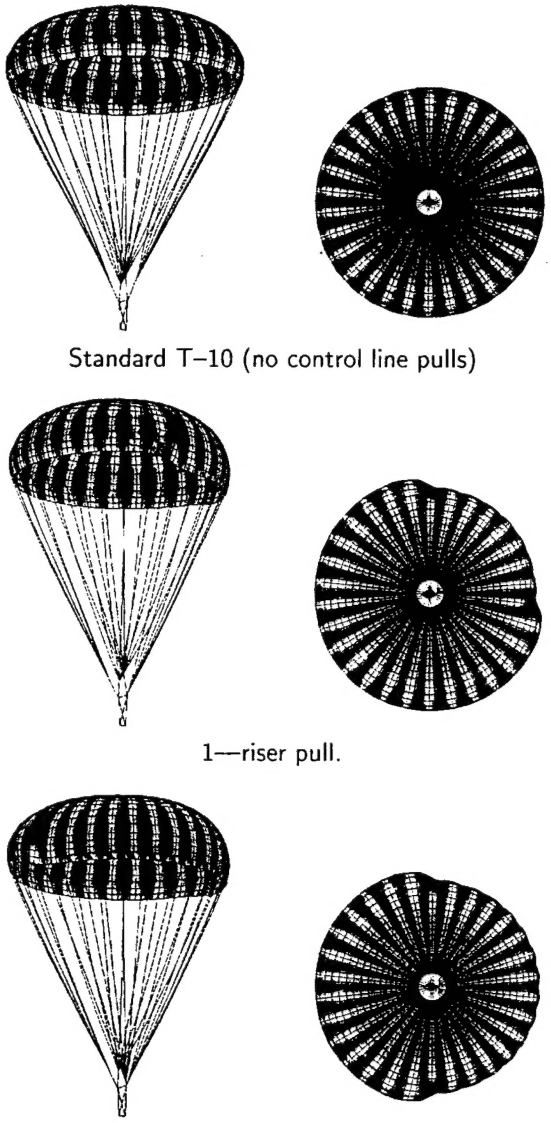

Figure 6. T–10 parachute during standalone SD simulation (maximum principal stresses).

As with the previous example, initial unsteady flow solutions are obtained for the fully-inflated configurations. Figure 7 shows the differential pressures at an instant during the stand-alone CFD simula-

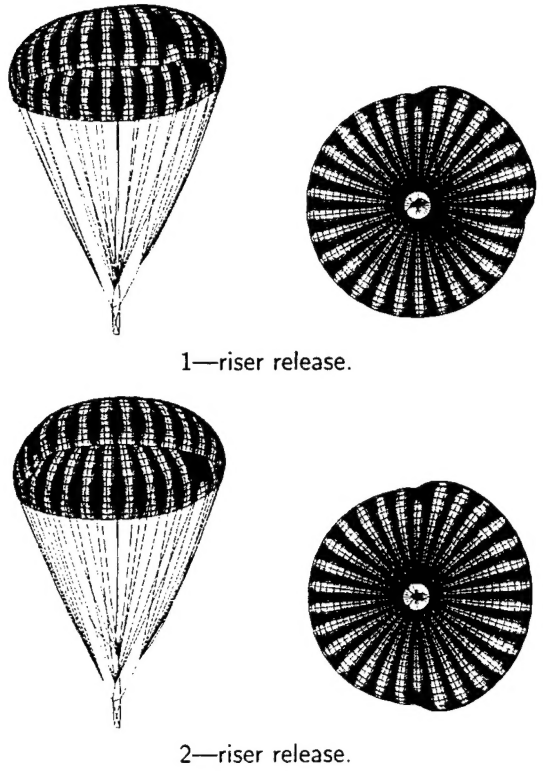

Figure 6. Continued

tions for the fixed canopy configurations. These flow solutions, along with the inflated configurations for the structure, will be used as a starting point for future FSI simulations.

The precise shape and motions for the parachute system with and without control line pulls is governed by a strong interaction between the structure and the fluid. Thus, accurate prediction of riser-slip behavior requires a FSI model. Results to corresponding FSI simulations are not yet available. Future simulations will address the FSI behavior for these riser-slip combinations.

CONCLUDING REMARKS

We have presented a strategy for carrying out 3-D simulations of parachute fluid-structure interaction has been presented and demonstrated for simulations of airdrop performance and control phenomena in terminal descent. The strategy is demonstrated to simulate the terminal descent behavior of a standard US Army personnel parachute system. Also, preliminary simulations are presented for the response of the parachute to a variety of "riser slips,"

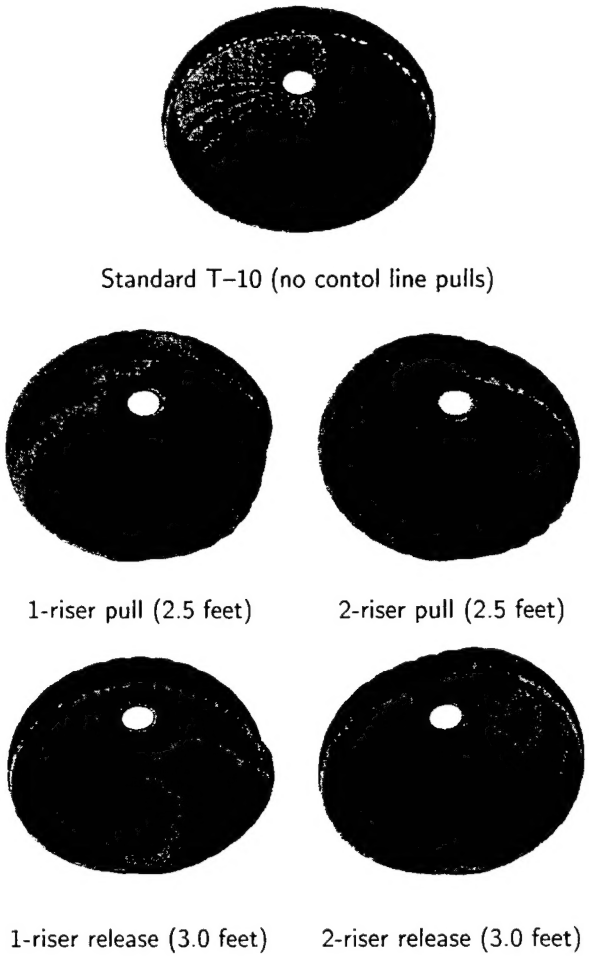

Figure 7. T–10 canopy during standalone CFD simulation (differential pressures).

which can provide the parachute system with limited maneuverability. Riser slips and control inputs to parachute systems (round, cruciform, parafoils, and other) are real applications for which this technology is being applied. The capability within DoD to reduce the life-cycle cost of such systems should be realized over the next several years as these modeling capabilities mature.

ACKNOWLEDGMENTS

This work was sponsored in part by AFOSR (contract number F49620–98–1–0214). The content does not necessarily reflect the position or the policy of the Government, and no official endorsement should be inferred.

References

1) S. Dellicker, R. Benney, S. Patel, T. Williams, C. Hewgley, O. Yakimenko, R. Howard and I. Kaminer, "Performance, Control, and Simulation of the Affordable Guided Airdrop System" *Proceedings of the AIAA Guidance, Navigaton, and Control Conference*, Aerodynamic Decelerator Session, AIAA-2000-4309, Denver, 2000.

2) T.E. Tezduyar, M. Behr and J. Liou, "A new strategy for finite element computations involving moving boundaries and interfaces – the deforming-spatial-domain/space-time procedure: I. The concept and the preliminary tests", *Computer Methods in Applied Mechanics and Engineering*, **94** (1992) 339–351.

3) T.E. Tezduyar, M. Behr, S. Mittal and J. Liou, "A new strategy for finite element computations involving moving boundaries and interfaces – the deforming-spatial-domain/space-time procedure: II. Computation of free-surface flows, two-liquid flows, and flows with drifting cylinders", *Computer Methods in Applied Mechanics and Engineering*, **94** (1992) 353–371.

4) M. Accorsi, J. Leonard, R. Benney and K. Stein, "Structural Modeling of Parachute Dynamics", *AIAA Journal*, **38** (2000) 139–146.

5) R.J. Benney, K.R. Stein, J.W. Leonard and M.L. Accorsi, "Current 3-D Structural Dynamic Finite Element Modeling Capabilities", *Proceedings of the 14th AIAA Aerodynamic Decelerator Systems Technology Conference*, San Francisco, 1997.

6) M. Accorsi, K. Lu, J. Leonard, R. Benney, and K. Stein, "Issues in Parachute Structural Modeling: Damping and Wrinkling", *Proceedings of the CEAS/AIAA 15th Aerodynamic Decelerator Systems Technology Conference*, AIAA-99-1729, Toulouse, France, 1999.

7) R. Benney, K. Stein, W. Zhang, M. Accorsi, and J. Leonard, "Controllable Airdrop Simulations Utilizing a 3-D Structural Dynamics Model", *Proceedings of the CEAS/AIAA 15th Aerodynamic Decelerator Systems Technology Conference*, AIAA-99-1727, Toulouse, France, 1999.

8) T.E. Tezduyar, M. Behr, S. Mittal, and A.A. Johnson, "Computation of Unsteady Incompressible Flows with the Stabilized Finite Element Methods–Space-Time Formulations, Iterative Strategies and Massively Parallel Implementations", *New Methods in Transient Analysis*, (eds. P. Smolinski, W.K. Liu, G. Hulbert and K. Tamma), AMD–Vol. 143, ASME, New York (1992) 7-24.

9) K.R. Stein, R.J. Benney, V. Kalro, A.A. Johnson and T.E. Tezduyar, "Parallel Computation of Parachute Fluid-Structure Interactions", *Proceedings of the 14th AIAA Aerodynamic Decelerator Systems Technology Conference*, San Francisco, 1997.

10) K. Stein, R. Benney, V. Kalro, T. Tezduyar, J. Leonard, and M. Accorsi, "Parachute Fluid-Structure Interactions: 3-D Computation", to appear in *Computer Methods in Applied Mechanics and Engineering.*

11) V. Kalro and T. Tezduyar, "A Parallel 3D Computational Method for Fluid-Structure Interactions in Parachute Systems", to appear in *Computer Methods in Applied Mechanics and Engineering*, Rice University MEMS Preprint 1999-029.

12) K. Stein, R. Benney, V. Kalro, T. Tezduyar, T. Bretl, and J. Potvin, "Fluid-Structure Interaction Simulations of a Cross Parachute: Comparisons of Numerical Predictions with Wind Tunnel Data", *Proceedings of the CEAS/AIAA 15th Aerodynamic Decelerator Systems Technology Conference*, AIAA-99-1725, Toulouse, France, 1999.

13) K. Stein, R. Benney, V. Kalro, T. Tezduyar, J. Leonard, and M. Accorsi, "3-D Computation of Parachute Fluid-Structure Interactions: Performance and Control", *Proceedings of the CEAS/AIAA 15th Aerodynamic Decelerator Systems Technology Conference*, AIAA-99-1714, Toulouse, France, 1999.

14) T.E. Tezduyar, "Stabilized Finite Element Formulations for Incompressible Flow Computations", *Advances in Applied Mechanics*, **28** (1991) 1–44.